Available online at www.sciencedirect.com
ScienceDirect
Journal of the European Ceramic Society 31 (2011) 1603–1609
www.elsevier.com/locate/jeurceramsoc

Fabrication of transparent $LaAlO_3$/t-ZrO_2 nanoceramics through controlled amorphous crystallization

Lin Mei [a,b], Gang He [a,b], Li-Li Wang [c], Guang-Hua Liu [a], Jiang-Tao Li [a,*]

[a] *Technical Institute of Physics and Chemistry, Chinese Academy of Sciences, Beijing 100190, China*
[b] *Graduate School of the Chinese Academy of Sciences, Beijing 100039, China*
[c] *Department of Materials Science and Engineering, University of Science & Technology Beijing, Beijing 100083, China*

Received 14 December 2010; received in revised form 20 February 2011; accepted 1 March 2011
Available online 13 April 2011

Abstract

Transparent nanoceramics are attracting more and more interests recently, while it is practically difficult to prepare by conventional sintering process because of undesirable grain growth. In this study a new method of amorphous sintering followed by controlled crystallization (ASCC) was developed, and transparent $LaAlO_3$/t-ZrO_2 nanoceramics were prepared as examples. Glass powders from Al_2O_3–La_2O_3–ZrO_2 (ALZ) were synthesized, sintered, and then converted to nanoceramics by post-heat-treatment. The processes of hot pressing and controlled crystallization were investigated in detail. The heat-treatment performed at 1200 °C for 2 h produced a transparent $LaAlO_3$/t-ZrO_2 nanoceramic with an average grain size of 40 nm. Due to the nanoscale microstructure, the composite showed a transparency up to 55% at 800 nm (1 mm thick), Vickers hardness of 19.05 GPa, and fracture toughness of 2.64 MPa $m^{1/2}$, respectively. It is expected to be a promising candidate for window materials.

Keywords: Nanoceramics; Amorphous crystallization; Grain growth; Optical properties; Mechanical properties

1. Introduction

Transparent ceramics, such as yttrium aluminum garnet (YAG), alumina (Al_2O_3) and alumina-magnesia spinel ($MgAl_2O_4$), have attracted increasing attentions because of their excellent mechanical strength (resistance to wear and bending), chemical and thermal stability (corrosion resistance), and optical properties (high refractive index), which provide wide applications ranging from high-pressure sodium and metal-halide lamps,[1,2] armor,[3] wave filter,[4] window materials[5,6] to lasers.[7]

Recently, most researches on transparent ceramics are focusing on tailoring the microstructure, e.g. the elimination of pores and refinement of grain size, in order to reduce light scattering and increase laser excitation efficiency.[8] It is significantly important for non-cubic systems because their optical properties are highly dependent on the grain size, such as α-Al_2O_3 with high anisotropic lattice ($c/a = 2.72$).[9] Fortunately, encouraging advance in optical performance of non-cubic transparent ceramics caused by the refinement of grain size has been well reported. For example, the in-line transmittance of Al_2O_3 ceramic greatly increases when the grain size is reduced into submicron scale, which makes translucent sample become transparent.[10] Based on the Rayleigh–Gans–Debye light-scattering theory, Apetz et al. developed a model to describe the light transmission properties of fine-grained fully dense ceramics.[11] This model explains the noteworthy transparency of the submicron-grained ceramics, and suggests that the light transmission of transparent ceramics will remarkably increase with the reduction of grain size. Furthermore, if the grain size can be reduced to nano-scale, the light transmission of transparent ceramics will be greatly improved.

While in conventional sintering of ceramic powders, the high temperature required for densification also promotes extensive grain growth, which makes it very difficult to prepare fully dense nanoceramics.[12] Hence, for preparing transparent nanoceramics, the key problem is to separate densification from grain growth. To do this, a possible approach is to make densification and grain growth take place through different mechanisms, which can offer the opportunity to control two processes separately. Recent researches indicate that coherent, dense,

* Corresponding author. Tel.: +86 10 82543695; fax: +86 10 82543695.
E-mail address: ljt0012@vip.sina.com (J.-T. Li).

0955-2219/$ – see front matter © 2011 Elsevier Ltd. All rights reserved.
doi:10.1016/j.jeurceramsoc.2011.03.004

amorphous bulk alloys and glasses can be successfully densified from amorphous powders by viscous flow within the kinetic window $\Delta T = T_g - T_s$, where T_g is the glass transition temperature and T_s is the starting crystallization temperature.[13,14] Based on these work, we develop a new method of amorphous sintering followed by controlled crystallization (ASCC), in which the amorphous powders were prepared, sintered via viscous flow, and then converted to transparent nanoceramics by heat-treatment.

Concentrated rare earth aluminates, $RAlO_3$, as well as R^{3+} ion as a dopant in $YAlO_3$ host lattice have roused interest as potential laser materials. Recently, $LaAlO_3$ powder has been synthesized via various methods,[15,16] while the transparent bulk material has not been reported except for single crystal because of the high birefringence of this extremely anisotropic lattice ($c/a = 2.44$). In the present work, transparent $LaAlO_3$-based nanoceramic was prepared by the ASCC method for the first time. The glass powder from Al_2O_3–La_2O_3–ZrO_2 was prepared, sintered and converted into transparent $LaAlO_3$/t-ZrO_2 nanoceramic via a controlled crystallization process. ZrO_2 was adopted to form a ternary system with high glass-forming ability,[17] and serviced as a nucleation agent. The feasibility of this method for other rare-earth-aluminate systems had also been demonstrated.

2. Experimental procedure

Raw materials used in this study included: Al_2O_3 (purity > 99.99%, $D_{V50} = 200$ nm, Dalian Luming Nanometer Material Co., Ltd.), La_2O_3 (purity ≥ 99.99%, $D_{V50} = 509$ nm, China Minmetals (Beijing) Research Institute) and m-ZrO_2 (purity ≥ 99.8, $D_{V50} = 46$ nm, Dongguan SG Ceramics Technology Co., Ltd.).

The experimental process was illustrated in Fig. 1. The powder mixtures with a molar composition of 53%Al_2O_3–20%La_2O_3–27%m-ZrO_2 (named hereafter as ALZ) were dispersed as an aqueous suspension with 1.5wt% polyvinyl alcohol (PVA, molecular weight 1700, purity ≥ 99.0%, Beijing Chemical Works) as binder, and spray dried into spherical particles. Spray dried agglomerates were feed into a C_2H_2/O_2 flame at a rate of 20 g/min, and then sprayed into water to prepare the ALZ glass microspheres, where the C_2H_2 flow rate was 20 l/min and the O_2 flow rate was 15 l/min. The flame was vertical to the water surface, and produced a combustion temperature up to 3200 °C. The particles were heated, melted and quenched into water to obtain a cooling rate of ~10^3 °C/s. The glass micropheres deposited at the bottom of a steel container were collected, dried and sieved. For hot-pressing, 5.0 g glass powder passed through 500 mesh was loaded into a graphite die (Ø20 mm), the internal surface of which was covered with a graphite sheet to avoid direct contact between the powder compact and the graphite die. The sintering temperature was elevated from room temperature to the final sintering temperature (about 900 °C) at 10 °C/min, and dwelled for several minutes to achieve the densification with the aid of a pressure exerted before the dwell. After cooled down, the obtained glasses were heat-treated at different temperatures (ranging from 900 to 1300 °C) to prepare the transparent nanoceramics.

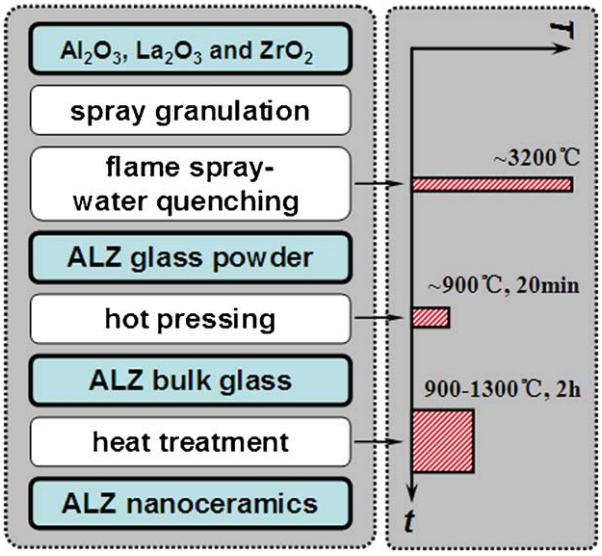

Fig. 1. Illustration of the studied experimental process. The right inset shows the temperature (T) and dwell time (t) used in each step. The T and t for hot pressing is relatively lower compared with conventional ceramic sintering.

The glass transition temperature (T_g) and starting crystallization temperature (T_s) of the glass microspheres were determined by a differential thermal analysis (DTA, NETZSCH STA 449C, Germany). Phase assemblage was identified by X-ray diffraction (XRD, D8 Focus, Bruker, Germany) using Cu Kα radiation. Microstructure was thoroughly characterized by scanning electron microscopy (SEM, Hitachi S-4300, Japan) and transmission electron microscopy (TEM, JEOL JEM 2100F, Japan). For the TEM observation, a thin sheet was mechanically polished to a thickness of 100 μm and further thinned by an Ar ion-milling machine. The in-line transmittance spectras were obtained using an UV–vis–NIR Spectrophotometer (Cary 5000, Varian, America) for 175–2000 nm and a Fourier Transform Infrared Spectra (FTIR; Excalibur 3100, Varian, America) for 2000 nm to 25 μm. All the samples were polished down to 1 mm thick. According to the mixture rule, the refractive index (n) of the ALZ glass is given by[18]

$$n = \phi_1 n_1 + \phi_2 n_2 + \phi_3 n_3 \quad (1)$$

where n_1, n_2 and n_3 are the refractive indexes of Al_2O_3, La_2O_3 and ZrO_2, respectively, Φ_1, Φ_2 and Φ_3 are the volume fractions of the respective components described above. Therefore, the n is 2.00. Based on these results, the theoretical transmittance (T_{th}) of the ALZ glass was calculated as 80% using the relations given in the literature.[11] The sample density was measured by Archimedes method, and the theoretical density can be calculated to be 4.56 g/cm^3 by an empirical equation[19]

$$\rho_{th} = 0.53 \cdot \frac{\sum(M_i \cdot x_i)}{\sum(V_i \cdot x_i)} \quad (2)$$

where M_i is molar weight (kg/mol), x_i is molar fraction (mol%), and V_i is paking density parameter (m^3/mol) for an oxide M_XO_Y. Based on the density variation, the degree of crystallization

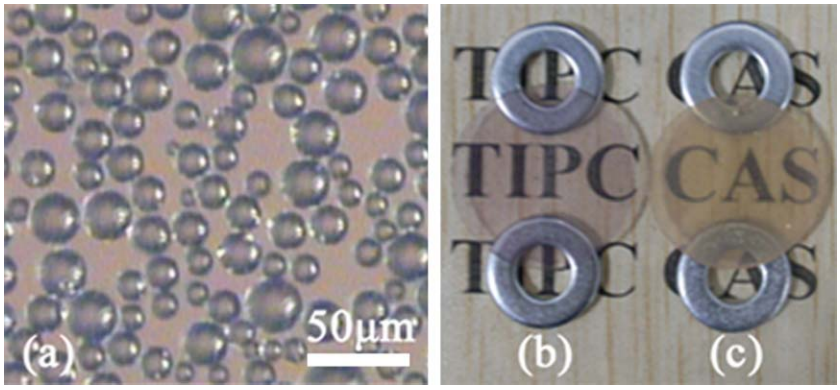

Fig. 2. (a) ALZ glass powders under an optical microscopy, (b) ALZ transparent glass and (c) $LaAlO_3$/t-ZrO_2 transparent nanoceramic prepared through crystallization at 1200 °C for 2 h. Both samples (b) and (c) are 1 mm thick and 0.6 cm above the text.

(α) of the heated sample was evaluated as reported in the literature.[20] Microhardness (H_v) and fracture toughness (K_{IC}) were measured using a microhardness machine (HXD-1000TM, Shanghai), and by application of 500gf (4.9 N) load on polished surface for 15 s.

3. Results and discussion

3.1. Preparation of ALZ glass powders by flame spray

For rare-earth-aluminate system, without including any glass forming oxides such as SiO_2, B_2O_3 and P_2O_5, both the high melt temperature and the required ultra-high cooling rate are serious obstacles for forming large bulk glass even by a laser-assisted melt-casting process.[21] In this study, the melting point of the ALZ system reached 1665 °C.[22] Although the flame spray process provided a high temperature up to 3200 °C, only the smaller particles could be heated to a temperature above the melting point during the supersonic spray process. As shown in Fig. 2(a), the ALZ glass powder with a particle size below 38.5 μm (−500 mesh) were fully spherical and transparent under an optical microscope because of the higher degree of melting and quenching. Differential Thermal Analysis (DTA) in Fig. 3 shows that the kinetic window (ΔT) of the ALZ amorphous microspheres was 816–895 °C. According to the empirical rule, the sintering temperature is generally chosen to be 20 °C lower than T_o so as to avoid devitrification.[23] Therefore, the optimal sintering temperature for the ALZ system was 875 °C, which is well located in the kinetic window for sintering.

3.2. Preparation of ALZ transparent glass by sintering

It is generally considered that the sintering of glass frit into bulk forms is realized by viscous flow within the kinetic window, while the densification rates are positively proportional to the applied pressure P according to the $d\rho/dt = 3P(1-\rho)/4\eta$, where η is the viscosity.[24] Thus, during the sintering process conducted at 875 °C, a pressure ranging from 30 to 90 MPa was applied to achieve full densification as soon as possible. The shrinkage behaviors are shown in Fig. 4. It is observed

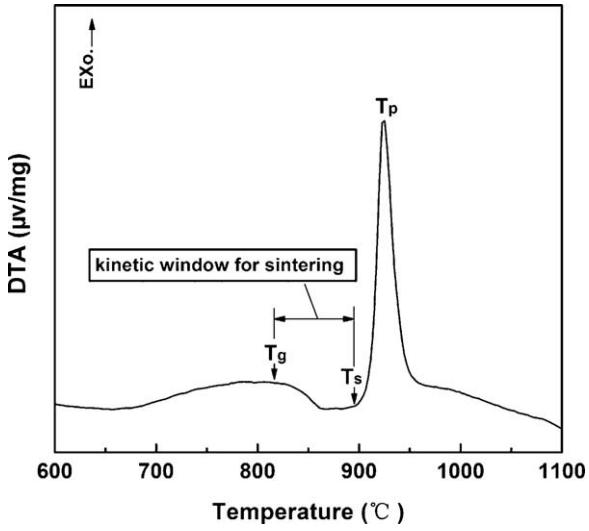

Fig. 3. DTA curve of ALZ glass powders at heating rate 10 °C/min.

that the shrinkage process consisted of three stages, including accelerating shrinkage, rapid shrinkage and shrinkage stagnation. The rapid shrinkage stage made a largest contribution up to 90% to the densification. Meanwhile, the applied pressure

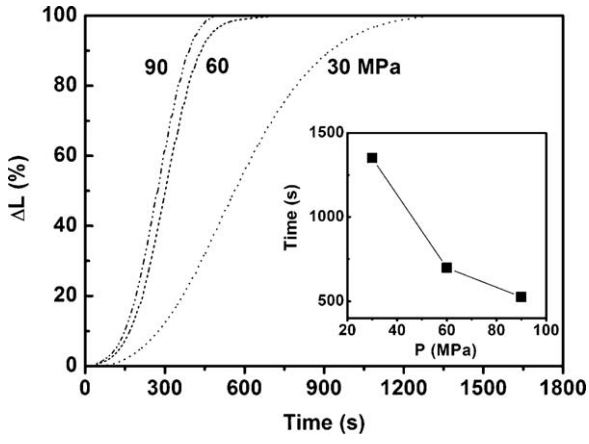

Fig. 4. Shrinkage behaviors of ALZ glass powders sintered at different pressures 30, 60 and 90 MPa. The inset shows the dependence of shrinkage time on applied pressure.

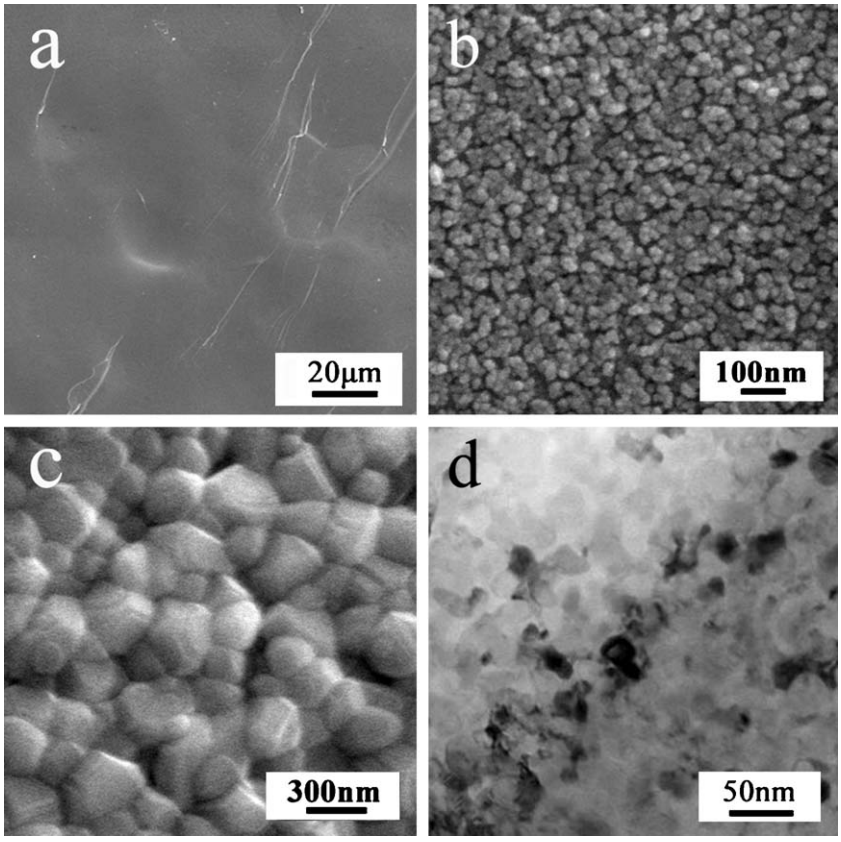

Fig. 5. SEM micrographs of the fracture surfaces of ALZ glass (a) and ceramics produced at 1200 °C (b) and 1300 °C (c) for 2 h. (d) TEM image of b.

accelerated the shrinkage rate dramatically. When the pressure reached 90 MPa, the time for full densification decreased from 1350 to 525 s, as observed in the inset of Fig. 4. The shorter dwell time is well benefic for avoiding the surface devitrification of glass microspheres, so as to aid the elimination of residual pores.

The ALZ glass sample sintered at 90 MPa is shown in Fig. 1(b). The density was measured as 4.55 g/cm^3, which reached 99.8% of the theoretical value. As shown in Fig. 5(a), the sintered bulk glass sample exhibited conchoidal fracture, and no obvious pores were found on the fracture surface. Meanwhile, the sample seemed to be a whole bulk, indicating that the interfaces of glass microspheres had disappeared by viscous flow. This is very different from the polycrystalline ceramics sintered at high temperatures. These results suggest that the higher pressure instead of temperature is essential to sinter the transparent glass. Fig. 6 shows that the ALZ glass had a transparency in a wide wavelength range of 265 nm to 6.54 μm, covering visible, near infrared and middle infrared regions. The transmittance of this sample reached 68% at 800 nm, and reached the maximum value of 75% in the range of 2.4–4.4 μm. Compared with the theoretical transmittance (80%), the loss should be attributed to the light scattering caused by residual pores, minor translucent and opaque glass microspheres. X-ray diffraction analysis (XRD) in Fig. 7 indicates that the sintered sample remained full amorphous, which is beneficial for the followed crystallization treatment to achieve desirable nano-sized grains.

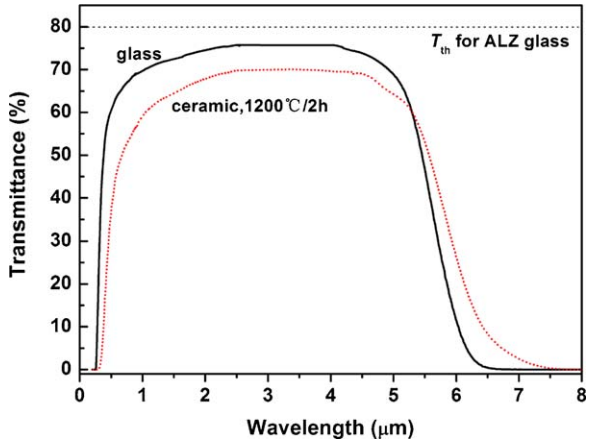

Fig. 6. Transmittance spectrums of ALZ glass (a) and $LaAlO_3$/t-ZrO_2 nanoceramic prepared through crystallization at 1200 °C for 2 h (b). The sample thickness is 1 mm.

3.3. Preparation of ALZ transparent nanoceramics by crystallization

Controlling the crystallization kinetics of amorphous bulk is of critical importance to obtain nano-sized ceramics, by optimizing the post heat-treatment conditions, such as heating temperature and time.[14] Therefore, the heat-treatment for the ALZ bulk glass was conducted in the temperature range of 900–1300°C for 2 h, and the influences of the heat-treatment

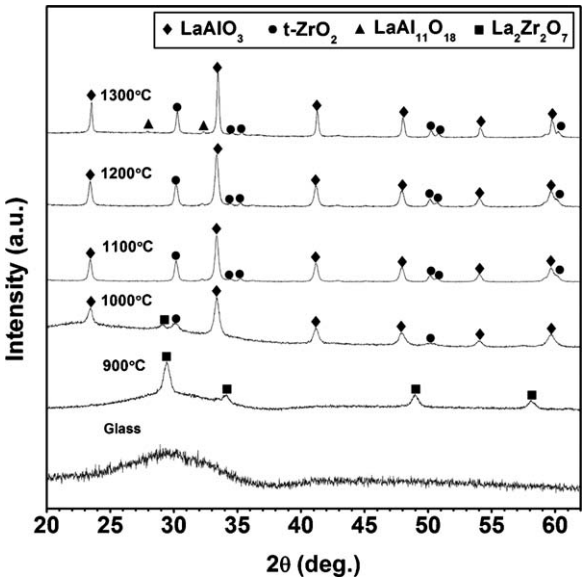

Fig. 7. XRD patterns of ALZ samples after heat-treatment at various temperatures. Indexed according to JCPDS cards: 85-848 ($LaAlO_3$), 80-965 (t-ZrO_2), 34-0467 ($LaAl_{11}O_{18}$) and 71-2363 ($La_2Zr_2O_7$).

temperature on crystallization behavior were thoroughly investigated.

Fig. 7 presented the XRD patterns of ALZ specimens after heat-treatment. It is noted that the sample treated at 900 °C precipitated a crystalline phase $La_2Zr_2O_7$. This should be attributed to the nucleation effect of ZrO_2.[25] The amount of ZrO_2 in this composition was considerably more than what is commonly used in glass–ceramic technology as a nucleation agent. The precipitation of plenty of fine compound $La_2Zr_2O_7$ renders heterogenenous nucleation sites and improves nanocrystallization. At 1000 °C, the diffraction peak of $La_2Zr_2O_7$ almost disappeared, and the following crystalline phases precipitated: $LaAlO_3$ and t-ZrO_2. As for the sample treated at 1100 and 1200 °C, except $LaAlO_3$ and t-ZrO_2, no new crystalline phase was detected. When the temperature increased to 1300 °C, minor $LaAl_{11}O_{18}$ appeared. However, the diffraction intensities of $LaAlO_3$ and t-ZrO_2 only increased slightly. This indicates that the crystallization process is almost complete.

Fig. 8 shows that both the density (ρ) and crystallization degree (α) of the samples increased dramatically with an increase in heat-treatment temperature. A complete crystallization was achieved at 1300 °C for 2 h, accompanied by a density increase from 4.55 to 5.34 g/cm^3. Notably, when the treatment was performed at 1200 °C for 2 h, the crystallization degree had reached 95.2 wt%, which suggests that the transition from glass to crystalline ceramic had been realized. XRD patterns in Fig. 7 also show that the sample heated at 1200 °C for 2 h mainly consisted of $LaAlO_3$ and t-ZrO_2 crystallines, and no amorphous characteristic was observed. Thus, the $LaAlO_3$/t-ZrO_2 nanoceramic was successfully prepared in this study. However, for traditional silicate system, only some nanophase glass–ceramics have been prepared by the crystallization method, that is, it is difficult to achieve a high degree of crystallization because of the different crystallization abilities of the multi-component systems.

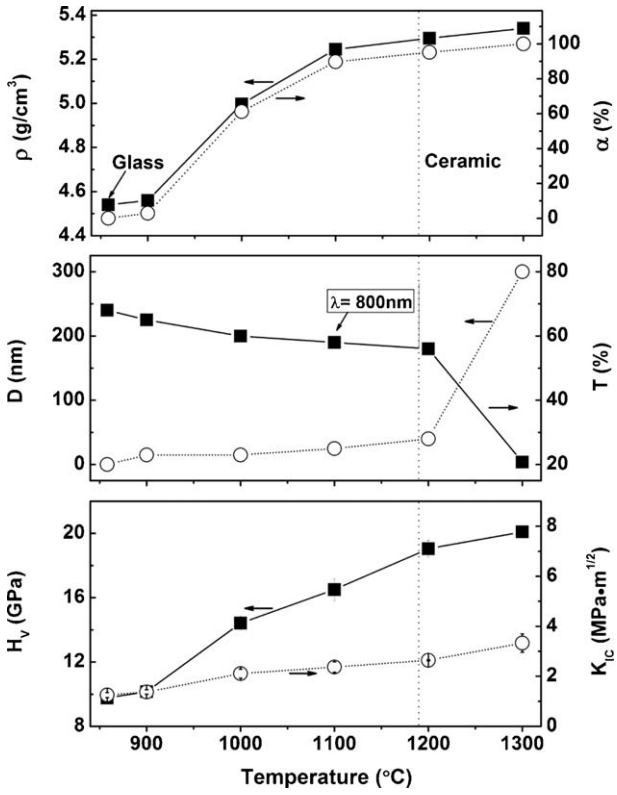

Fig. 8. Effects of heating temperature on density ρ and crystallization degree α (a), grain size D and transmittance T (b), and Vickers hardness H_V and fracture toughness K_{IC} (c).

Scanning electron microscopy (SEM) and Transmission electron microscopy (TEM) observations on fracture surface also provide good insight into the processes occurring during crystallization, as shown in Fig. 5(b–d). The $LaAlO_3$/t-ZrO_2 ceramic obtained at 1200 °C exhibited a compact surface, suggesting that almost no residual glass phase remained in the matrix. TEM image in Fig. 5(d) shows that no obvious pores were observed despite a great volume shrinkage took place during the controlled crystallization process. When the heating temperature was elevated to 1300 °C, the fracture surface of the sample appears to be intergranular, which directly indicated that the sample had been completely crystallized. This is well consistent with the analysis results above.

Controlled grain growth was also achieved by controlled crystallization via modifying the heating temperature from 900 to 1300 °C. As shown in Fig. 8(b), the average grain size (D) remained below 40 nm until the heating temperature was elevated to 1200 °C, leading to a slight transparency loss due to the neglectable light scattering from grain boundaries. So the $LaAlO_3$/t-ZrO_2 ceramic obtained at 1200 °C (Fig. 1(c)) showed a transparency up to 70% in the infrared region, which is almost the same as that of the parent glass, while in the visible region the transmittance at 800 nm decreased from 68% to 55% because of the presence of nanocrystals (Fig. 6). When the heating temperature was 1300 °C, the grain grew quickly to 300 nm, and the sample became opaque. According to the Rayleigh–Gans–Debye light-scattering theory, the optical properties of non-cubic systems are highly dependent on the

grain size because of the light scattering from birefringence.[11] For example, if the grain size is in micrometer scale, the Al_2O_3 ceramics ($c/a = 2.72$) are translucent. While if the grain size can be reduced to nano-scale, the transmittance will be improved to the theoretical value. In this study, the transmittance of $LaAlO_3$/t-ZrO_2 nanoceramic exhibited a similar dependence on the grain size as described above. Meanwhile, the shrinkage-induced pores and cracks are liable to form during crystallization, although these defects were not detected by SEM and TEM analysis. This could be one more reason for the opacity of the completely crystallized samples obtained at 1300 °C.

In addition, the heat-treated ALZ samples exhibited enhanced Vickers hardness (H_V) and fracture toughness (K_{IC}) (Fig. 8(c)). Compared with the sintered basic glass, the transparent $LaAlO_3$/t-ZrO_2 nanoceramic obtained at 1200 °C had an almost doubled Vickers hardness of 19.05 GPa and fracture toughness of 2.64 MPa $m^{1/2}$, respectively. This remarkable improvement should be attributed to the increased density and crystallization degree, and the nanoscale microstructure.

It is well known that optical sapphire (Al_2O_3), spinel ($MgAl_2O_4$) and AlON ($Al_{23-1/3x}O_{27+x}N_{5-x}$, $0.429 < x < 2$) have widely been used as window materials because of their excellent combined properties.[26] Of these, AlON transparent polycrystalline ceramic is an extremely durable material with mechanical and optical properties similar to sapphire, for example, a Vickers hardness of 16.00 GPa and fracture toughness of 2.40 MPa $m^{1/2}$, respectively.[27] In this work, the prepared transparent $LaAlO_3$/t-ZrO_2 nanocomposite exhibited more attractive mechanical properties, which suggest a potential application in window materials. However, more efforts should be made to improve the optical properties of $LaAlO_3$/t-ZrO_2 nanocomposite by optimizing the new developed process.

4. Conclusions

Transparent $LaAlO_3$/t-ZrO_2 nanoceramics were successfully prepared by the new developed method of amorphous sintering followed by controlled crystallization. Glass powders from Al_2O_3–La_2O_3–ZrO_2 were synthesized, sintered by viscous flow, and then converted to transparent $LaAlO_3$/t-ZrO_2 nanoceramics by post-heat-treatment. In the densification of glass powders, the higher pressure instead of temperature was essential to sinter transparent glass. The increased heat-treatment temperature led to a remarkable increase in density, crystallization degree, grain size and mechanical properties, while a decrease in transparency. The heat-treatment performed at 1200 °C for 2 h produced transparent $LaAlO_3$/t-ZrO_2 nanoceramic with an average grain size of 40 nm. Due to the reduced light scattering from birefringence, the transmittance of $LaAlO_3$/t-ZrO_2 nanoceramic (1.0 mm thick) was up to 55% at 800 nm. Meanwhile, the transparent $LaAlO_3$/t-ZrO_2 nanoceramic exhibited a Vickers hardness of 19.05 GPa, and fracture toughness of 2.64 MPa $m^{1/2}$, respectively.

Compared with conventional sintering process, this technique provides a new route to prepare transparent nanoceramics by separating the densification stage from grain growth, in which the grain size is easily controlled by modifying the crystallization temperature. Hence the method is also applicable to other rare-earth-aluminate systems which can provide amorphous powders with a wider kinetic window for densification.

Acknowledgments

This work was supported by the National Natural Science Foundation of China under grants No. 50772116 and 50932006 (Key Project).

References

1. Krell A, Blank P, Ma HW, Hutzler T, van Bruggen MPB, Apetz R. Transparent sintered corundum with high hardness and strength. *J Am Ceram Soc* 2003;**86**:12–8.
2. Tu J. Influence of mount structure on performance of ceramic metal halide lamps. *IEEE Trans Ind Appl* 2008;**44**:1987–92.
3. Klement R, Rolc S, Mikulikova R, Krestan J. Transparent armour materials. *J Eur Ceram Soc* 2008;**28**:1091–5.
4. Morita K, Kim BN, Yoshisa H, Hiraga K. Spark-plasma-sintering condition optimization for producing transparent $MgAl_2O_4$ spinel polycrystal. *J Am Ceram Soc* 2009;**92**:1208–16.
5. Krell A, Klimke J, Hunzler T. Advanced spinel and sub-μm Al_2O_3 for transparent armour applications. *J Eur Ceram Soc* 2009;**29**:275–81.
6. Schneider H, Schreuer J, Hildmann. Structure and properties of mullite—a review. *J Eur Ceram Soc* 2008;**28**:329–44.
7. Ikesue A, Aung YL. Ceramic laser materials. *Nature* 2008;**2**:721–7.
8. Messing GL, Stevenson AJ. Toward pore-free ceramics. *Science* 2008;**322**:383–4.
9. Stuer M, Zhao Z, Aschauer U, Bowen P. Transparent polycrystalline alumina using spark plasma sintering: effect of Mg, Y and La doping. *J Eur Ceram Soc* 2010;**30**:1335–43.
10. Rayashi K, Kobayashi O, Toyoda S, Morinaga K. Transmission optical properties of polycrystalline alumina with submicron grains. *Mater Trans JIM* 1991;**32**:1024–9.
11. Apetz R, van Bruggen MPB. Transparent alumina: a light-scattering model. *J Am Ceram Soc* 2003;**86**:480–6.
12. Kingery WD, Bowen HK, Uhlmann DR. *Introduction to ceramics*. 2nd ed. New York: Wiley & Sons; 1976.
13. Rosenflanz A, Frey M, Enderson B, Richards E, Schardt C. Bulk glasses and ultrahard nanoceramics based on alumina and rare-earth oxides. *Nature* 2004;**430**:761–4.
14. Lu K. Synthesis of nanocrystalline materials from amorphous solids. *Adv Mater* 1999;**11**:1127–8.
15. Hreniak D, Stręk W, Dereń P, Bednarkiewicz A, Łukowiak A. Synthesis and luminescence properties of Eu^{3+}-doped $LaAlO_3$ nanocrystals. *J Alloys Compd* 2006;**408–412**:828–30.
16. Kuo CL, Chang YH, Wang MC. Crystallization kinetic of lanthanum monoaluminate ($LaAlO_3$) nanopowders prepared by co-precipitation process. *Ceram Int* 2009;**35**:327–32.
17. Sakamoto N, Araki S, Yoshimura M. Fabrication of nanocomposite ceramic by crystallization of rapidly solidified eutectic melts. *J Am Ceram Soc* 2009;**92**:S157–61.
18. Heller W. Remarks on refractive index mixture rules. *J Phys Chem* 1965;**69**:1123–9.
19. Inaba S, Fujino S. Emperical equation for calculating the density of oxide glass. *J Am Ceram Soc* 2010;**93**:217–20.
20. Karamanov A, Pelino M. Evaluation of the degree of crystallization in glass–ceramics by density measurements. *J Eur Ceram Soc* 1999;**19**:649–54.
21. Richard Weber JK, Abadie JD, Hixson AD, Nordine PC, Jerman GA. Glass formation and polyamorphism in rare-earth oxide-aluminum oxide compositions. *J Am Ceram Soc* 2000;**83**:1868–72.

22. Lakiza SM, Lopato LM. Phase diagram of the Al_2O_3–ZrO_2–La_2O_3 system. *J Eur Ceram Soc* 2005;**25**:1373–80.
23. Cheng JS, Li H, Tang LY, He F. *Glass–Ceramics*. Beijing: Chemical Industry Press; 2007.
24. Vasilos T. Hot Pressing of Fused Silica. *J Am Ceram Soc* 1960;**43**:517–9.
25. Banijamali S, Eftekhari Yekta B, Rezaie HR, Marghussian VK. Crystallization and sintering characteristics of CaO–Al_2O_3–SiO_2 glasses in the presence of TiO_2, CaF_2 and ZrO_2. *Thermochim Acta* 2009;**488**:60–5.
26. Sands JM, Fountzoulas CG, Gilde GA, Patel PJ. Modelling transparent ceramics to improve military armour. *J Eur Ceram Soc* 2009;**29**:261–6.
27. McCauley JW, Patel P, Chen MW, Gilde G, Strassburger E, Paliwal B, et al. AlON: a brief history of its emergence and evolution. *J Eur Ceram Soc* 2009;**29**:223–36.